# Study on effective band of advanced microwave scanning radiometer (AMSR) for observing first year sea ice in the Okhotsk Sea by airborne microwave radiometer (AMR)

Masashige Nakayama[*1], **Fumihiko Nishio**[*2], Tomonori Tanikawa[*2]
Kohei Cho[*1] and Haruhisa Shimoda[*1]

[*1] Tokai University Research and Information Center
2-28-4, Tomigaya, Shibuyaku-ku, Tokyo, 151-0063, Japan
[*2] Hokkaido University of Education, Kushiro campus
1-15-55, Shiroyama, Kushiro-shi, Hokkaido, 085-0826, Japan

**Abstract:**

It is very important for monitoring the interannual variability of sea ice extents in the Okhotsk Sea because the global warming has firstly appeared around the Okhotsk Sea, locating around the southernmost region of sea ice cover in the Northern Hemisphere. In order to develop the sea ice concentration algorithm by microwave sensors onboard satellite, electromagnetic properties of sea ice in the Okhotsk Sea, therefore, were observed by airborne microwave radiometer (AMR), which has the same frequencies as AMSR (Advanced Microwave Scanning Radiometer), ADEOS-II, launching on November, 2000.

On this study, it is discussed how to make the image of AMR-EFOV and the video image with nadir angle under flight at the same time, and superimpose the brightness temperature data by AMR-EFOV on the video mosaiced images. For comparing SPOT image, it is clearly that the variation of brightness temperature is small in 89GHz V-pol without the sea ice types and increase at the lower frequency-band.

Key words : sea ice extent, passive microwave radiometer, ADEOS-II/AMSR

## INTORODUCTION

SSM/I (Special Sensor Microwave/Imager) in DMSP (Defense Meteorological Satellite Program) is observing to earth environmental in now. On November 2000, ADEOS-II/AMSR (Advanced Earth Observing Satellite － Ⅱ / Advanced Microwave Scanning Radiometer) will be launched by NASDA. On end, EOS-PM1 / AMSR-E will be launched by NASA. Therefore, the observing resolution is advanced and frequency-bands of observation are increased. In addition, the variation cycle of observed object in a day is will used in the algorithm for ADEOS-II and EOS-PM1 observed in AM and PM respectively.

For more over two decades the monitoring of sea ice using satellite microwave radiometer have been continued. But, the current algorithms for sea ice concentration (NASA Team Algorithm[1)] and Bootstrap Algorithm[2)]) is not enough accuracy in the low latitude area,[3)] a kind of Okhotsk Sea. Although, it is important to monitor the sea ice extent in Okhotsk Sea, because the result of calculation, using GCM model, indicated that the sea air temperature will increase in Okhotsk Sea more than another sea. It will be possible to catch the

progress of global warming and to estimate the local climate change around countries. In this study, the sea ice property of the microwave signature is observed using AMR (Airborne Microwave Radiometer). AMR can observe microwave signature of the object as brightness temperature in same band of AMSR.

## SENSOR and STUDY AREA

The Airborne Microwave Radiometer (AMR) is a NASDA–developed airborne instrument in the ADEOS-II/AMSR program. AMR has the observation band from 6.925GHz to 89.0GHz and horizontally / vertically polarization (H-pol / V-pol). The data used in this study is obtained on a Beachcraft-200 aircraft over the sea ice in Okhotsk Sea. AMR observation concept is shown in Fig. 1. Table 1 is AMR parameter specifications.

AMR is point sensor of H-pol and V-pol alternately. The integration time is 1.33 second. The Effective Filed of View (EFOV) area is different each frequency bands and polarization. Therefore, VTR images ware taken at a just under the airplane for the auxiliary data. The study area is shown Fig. 2 and the day of observation is Feb, 17 1996. Plate 1 is SPOT/HRV image at the AMR observation day.

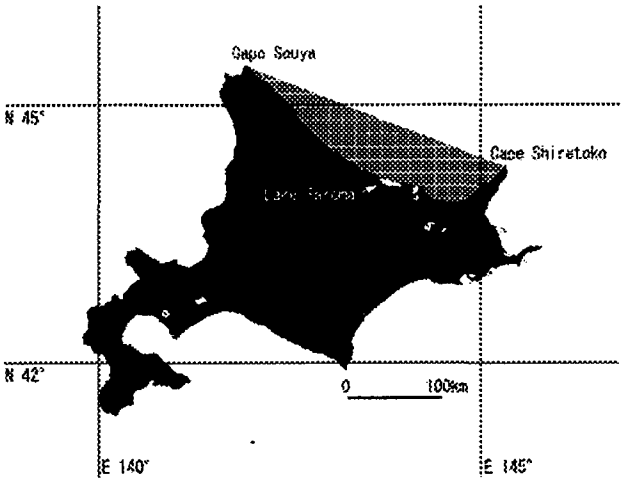


Fig. 2 The observation area is part of meshed. Lake Saroma connects up Okhotsk Sea by way of two mouth. The concentration of salt in water is almost same as the open sea. Therefore, the ice of Lake Saroma is regarded as the sea ice floe in the open sea.

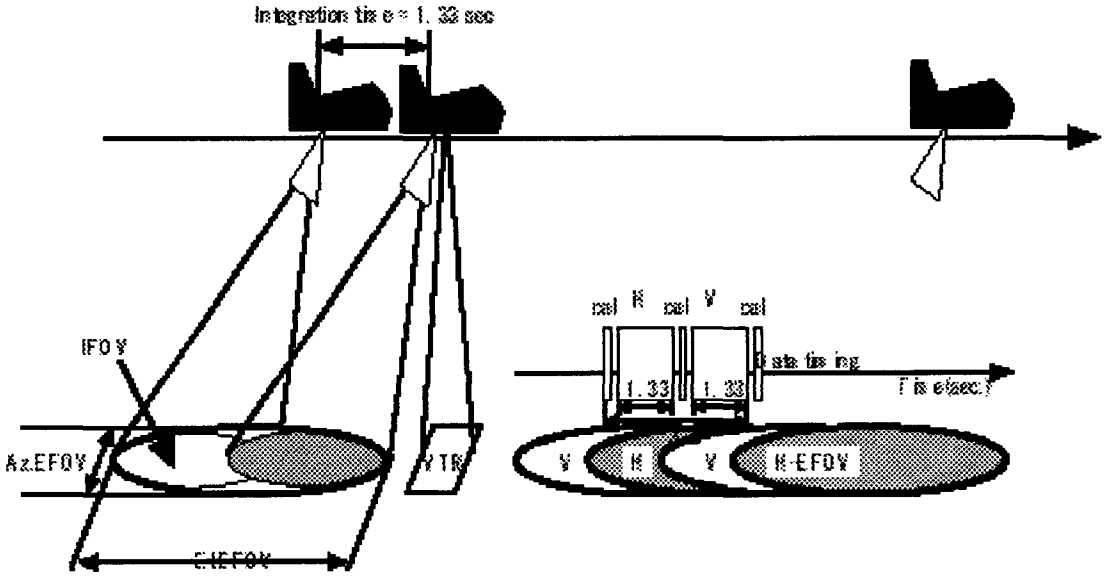


Fig. 1 Projection of the AMR IFOV and VTR camera on the observation surface. The band of horizontally and vertically polarized wavelength is observed alternately. The integration time is 1.33 second for each band. The VTR camera is set up with nadir angle to see the surface of sea ice.

## DATA ANALYSIS

The AMR is point sensor without a mechanics of driving, so the data is a profile of the one dimension along the flight course. It could not to obtain the two dimension data like a image. However, the sea ice moves momentarily. It is necessary for comparison of the AMR's data and the surface property to take information of an observed surface. Therefore, it was developed that how to the effective field of view (EFOV) images of AMR are obtained from VTR images for each frequency-band and H-pol / V-pol. The VTR image is taken at the same time of the flight observation using AMR.

First, the mosaiced images of the observation were made from the VTR images. The VTR image has 30 frames at one second, that is to show 30 fps. The images of VTR were filed as the movie through the A/D converter. At this point, the frame rate of movie files is changed as the flight altitude more over 90% of a lap between image to image to calculate a distance of images. The software to make a mosaiced image from a movie image was developed for the another study.[4] How to calculate the center position on the mosaiced image is shown in the following method.

It is possible to make the coordinates using observation time, if $T_1$ of the time, observed at the first frame of VTR, is decided. This coordinate is the one dimension along the flight direction. It was said the observation times coordinates in this study. If the average of flight speeds is shown v (m/s) between the first frame and the number of n frame, the distance of movement, Dn (m), is shown

$$Dn = v(Tn - T_1) \quad (1)$$

where $T_1$ and Tn is the observed time at the first frame and the number of n frames of the movie file from VTR. Moreover, it is possible to set the observation times coordinates dividing the both sides of (1) by the speed of flight v. Based on this method, the center of AMR-EFOV at the observation time is shown Tn'.

$$Tn' = Tn - h \cdot \tan \alpha / v \quad (2)$$

Where Tn is the observation time at the same time, h is the flight altitude and $\alpha$ is the incident angle of the sensors. Fig. 4 is a sample image of AMR-EFOV respectively the frequency-band. Then, the property of sampled sea ice at the brightness temperature is investigated by comparison the SPOT image.

The time of observation using AMR is from 9:31 to 12:26, the scene center time of SPOT image about Plate 1 is 10:05. In the Plate 1, the narrow lines are mosaiced images which scale fits into a resolution of SPOT image. The sea ices, selected from SPOT image overlapped mosaiced image areas, are seven sampled. There are shown A', B – G and Lake of Saroma in Fig. 5 at each frequency-band and polarization respectively. In this result of Fig. 5, the values of sample A' are calculated using a regression line, because the area of sampled A' consist of small sea ices. It is size about 1m.

Table 1. Specification of the AMR. The width of beam is reversed (El.) and (Az.) in the vertically polarized wavelength.

| Center frequencies (GHz) | 6.925 | 10.65 | 18.7 | 23.8 | 36.5 | 89.0 |
|---|---|---|---|---|---|---|
| Integration time (sec) | 1.33 | | | | | |
| Polarization | Vertical and horizontal for all channels | | | | | |
| Beamwidth Az. | 10.8 | 9.0 | 6.6 | 5.5 | 6.3 | 6.0 |
| (3db deg.) El. | 12.3 | 10.0 | 7.9 | 6.3 | 7.2 | 6.9 |
| Sampling Rate (s) | 3.2 | | | | | |

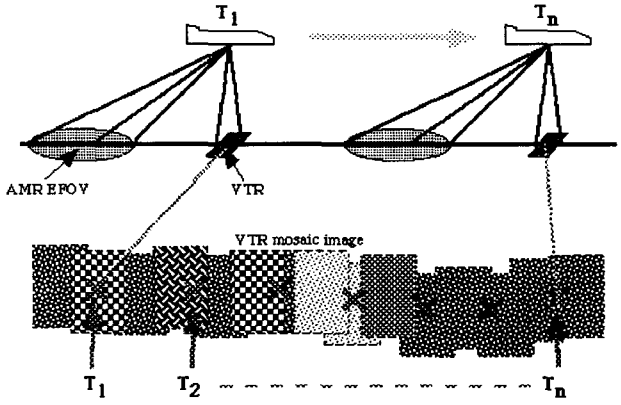


Fig. 3 Concept image of the coordinate using the observation time. The coordinate of observation time is set at the mosaiced image along the flight direction. Therefore, it is possible to locate EFOV of AMR in the mosaiced image.

Fig. 4 Sample images of AMR-EFOV cutting from the mosaiced image. The ellipse of the small size (translucent) is IFOV of AMR.

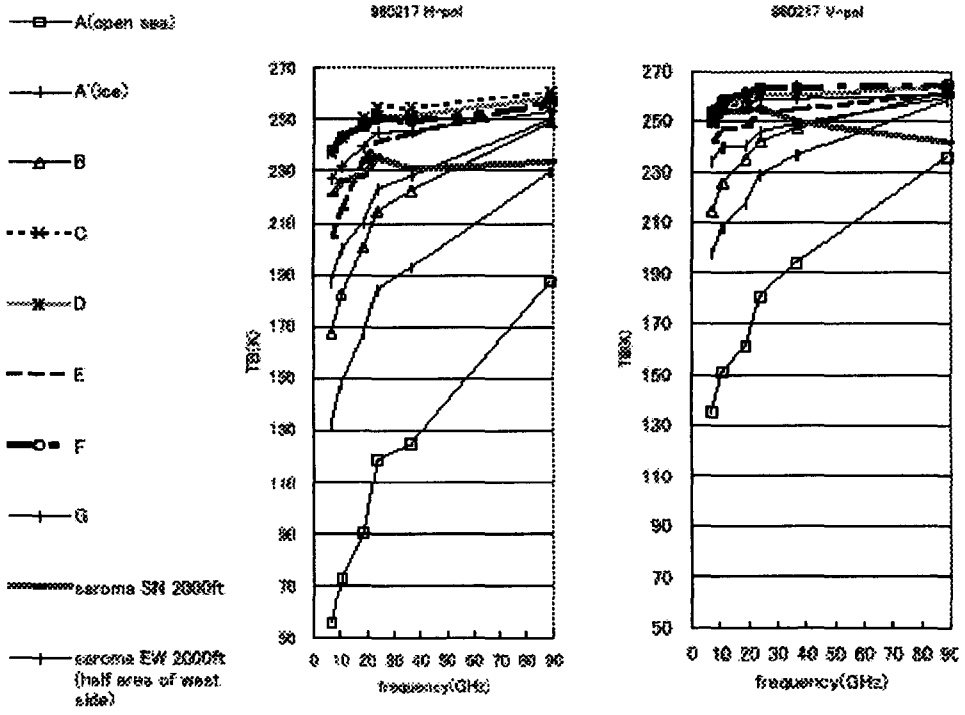


Fig. 5 Property of the brightness temperature to the frequency at the each sampling sea ice.

## RESULTS

In this result of Fig. 5, there is different point in a property of SAROMA-SN. Only SAROMA-SN, the brightness temperature in 36.5GHz and 89.0GHz are decrease. In the another sample, included the open water, the brightness temperature increase with frequency. This trend is opposite in the multiyear ice of the polar area.[5] Another point, the sea ice and open water are separated clearly in the 89.0GHz V-pol without SAROMA-SN. Therefore, it is calculated that (a) the different of the brightness temperature between the sea ice of maximum value and the open water, (b) the range of variation between the maximum and minimum of sea ice brightness temperature (H-pol : C – A', V-pol : F – A'), (c) the ratio of (a) to (b). The result is shown in Fig. 6. The values of (c) in Fig.6 are shown the intensity of the sea ice variation. In 89.0GHz V-pol, it is independence from different of sea ice property, because this value is minimum.

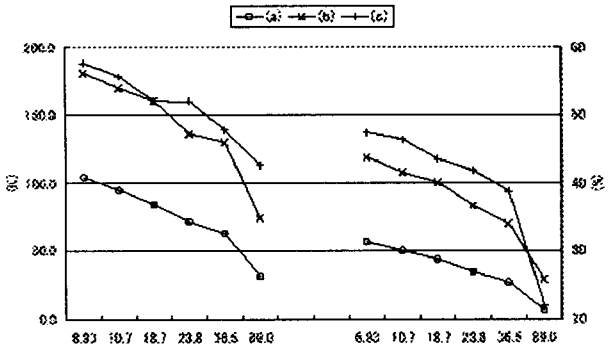

Fig. 6 Variation of dynamic rage at the brightness temperature between the sea ice and the open water.

## SUMMARY

The brightness temperatures of several sea ice types over the 6.925GHz to 89.0GHz range with horizontally and vertically polarization using the airborne microwave radiometer. The properties of brightness temperature at the initial stage of a generating sea ice are developed comparing SPOT image. These results shown the range of brightness temperature of the sea ice is increase at the lower frequency-band and it is minimum at 89.0GHz V-pol. Whereas SSM/I has the observation bands between 19.35GHz to 85.5GHz, AMSR extend between 6.925GHz to 89.0GHz. It is expectation for the monitoring of sea ice at the initial stage of a generating to improve the accuracy.

## Acknowledgments

This work was supported by contracts from NASDA, the collaboration title is the development of the sea ice concentration and classification algorithm for AMSR in Okhotsk sea. The authors extend their thanks to participants.

## REFERENCES

1) Gloersen, P. and D. J. Cavalieri, 1986, Reduction of weather effects in the calculation of sea ice concentration from microwave radiances. J. Geophys. Res., 91(C3), 3913-3919.

2) Comiso, J. C, 1995, SSM/I ice concentrations using the Bootstrap algorithm, NASA Report 1380.

3) Comiso, J. C., D. J. Cavalieri, C. L. Parkinson, and P. Gloersen, 1997, Passive Microwave Algorithms for Sea Ice Concentration : A Comparison of Two Techniques, Remote Sens. Environ., 60, pp.357-384, 1997.

4) Svendsen, E., Kloster, K., Farrelly, B., Johannessen, O. M., Johannessen, J. A., Campbell, W. J., Gloersen, P., Cavalieri, D., and Matzler, C., 1983, Norwegian remote sensing experiment: evaluation of the Nimbus 7 scanning multichannel microwave radiometer for sea ice research, J. Geophys. Res., 88 : 2781-2792.

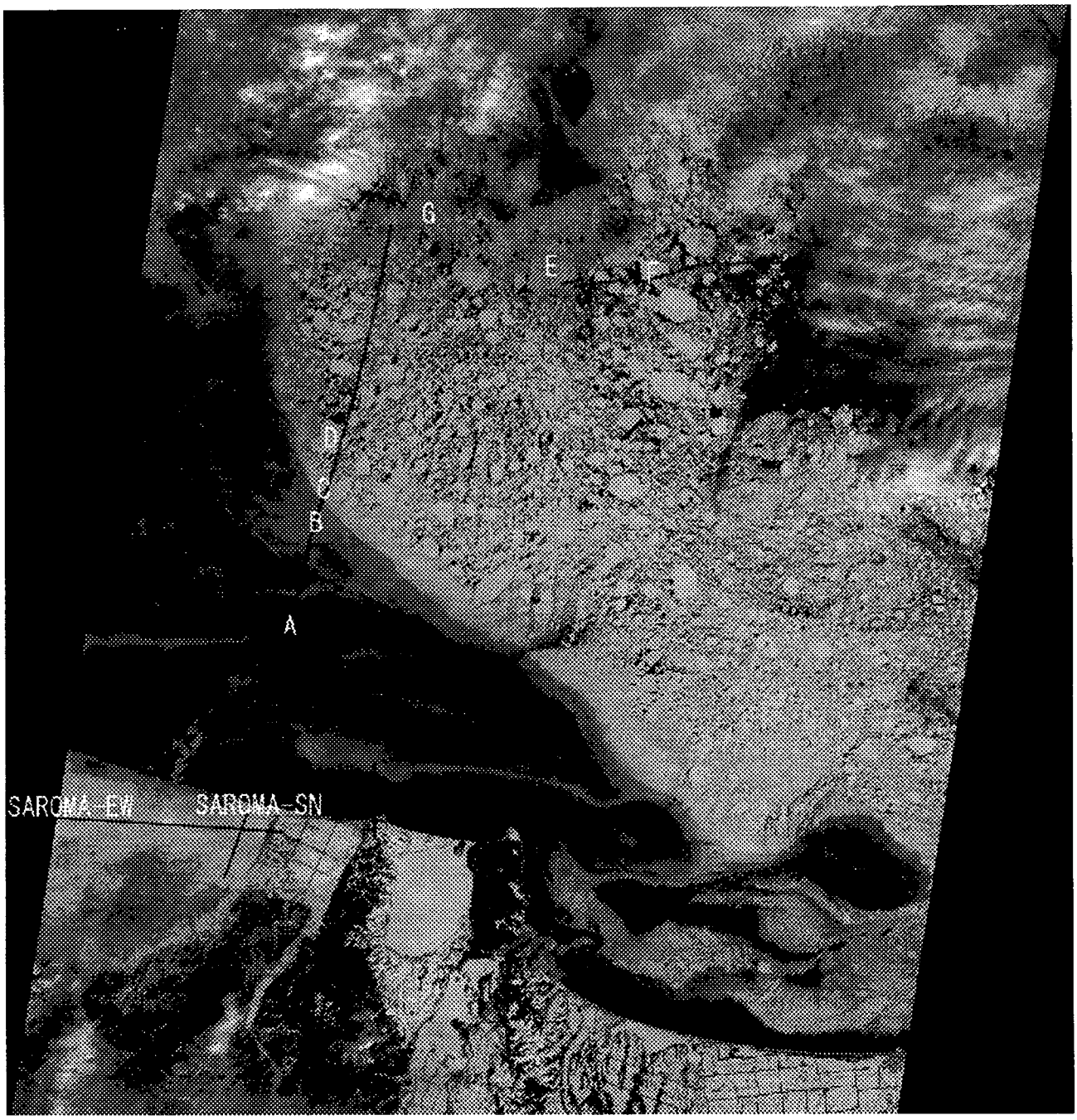


Plate 1 SPOT image at the same day of the observation using AMR.